Sea-level responses to rapid sediment erosion and deposition in Taiwan

Gregory A. Ruetenik[1], Ken L. Ferrier[1], Jessica R. Creveling[2], Matthew Fox[3]

[1] Department of Geosciences, University of Wisconsin, Madison

[2] College of Earth, Ocean, and Atmospheric Sciences, Oregon State University, Corvallis, OR

[3] Department of Earth Sciences, University College London, London, UK

Key words: Sea level, Sediment, Taiwan, Erosion

Abstract

Numerous studies have shown that sediment deposition can perturb sea level by several meters over millennial timescales by modifying the gravity field, crustal elevation, and sediment thickness. Relatively few studies have focused on the complementary role of erosion on sea-level change despite its effects on the same quantities, partly because many rapidly eroding mountains are too far from shorelines to strongly perturb sea level at the coast. Taiwan, a mountainous island eroding rapidly within tens of km of the coast, offers an opportunity to investigate the joint influences of rapid onshore erosion and rapid offshore deposition on sea-level change. Here we develop a sediment loading history for Taiwan since the previous interglacial (~120 ka) by compiling published erosion and deposition rate measurements and by applying a geometric marine sediment deposition and compaction model for sites without deposition rate measurements. We use the resulting sediment redistribution history to drive sea-level responses in a gravitationally self-consistent sea-level model. Our simulations show that the effects of rapid onshore erosion outweigh the effects of rapid offshore deposition along Taiwan's east coast.

Along the east coast of Taiwan, sediment redistribution induces rapid sea-level fall, a response that differs in sign from the coastal sea-level rise induced by rapid sediment redistribution in many other river systems around the world. The spatial extent of the modeled sea-level fall is sensitive to the Earth model, particularly the effective elastic thickness of the lithosphere, a sensitivity that we describe in further detail in the Discussion. These results suggest that sediment redistribution could have generated sea-level changes of >10 meters on the east coast of Taiwan since 10 ka and >100 m since 120 ka. This can account for some of the discrepancy between observed and modeled paleo-sea-level marker elevations, which reduces estimates of tectonically driven rock uplift rates inferred from the elevation differences between paleo-sea-level markers and modeled sea level. This highlights the importance of accounting for erosional unloading in interpretations of paleo-sea-level reconstructions and associated estimates of tectonically driven uplift rates.

1. Introduction

Rising sea level threatens low lying areas that contain about 10% of the world's population (Nicholls and Cazenave, 2010) and motivates efforts to understand the drivers of sea-level (SL) change. One of the most useful predictors of future sea-level change is the past sea-level record, which can be inferred from the elevations and ages of paleoshorelines and marine deposits, each of which record the cumulative sea-level change at a point in space since a given time (Rovere et al., 2014). However, reconciling these local sea-level indicators with proxies for global paleo-sea level, such as $\delta^{18}O$ in deep-sea benthic foraminifera (Lisiecki and Raymo, 2004; Doar and Kendall, 2014), is complicated by regional variations in sea level induced by viscoelastic deformation of the solid Earth in response to changes in loading of water, ice, and sediment (Haskell, 1935; Milne et al., 2001; Dalca et al., 2013), crustal uplift and subsidence due to tectonics and dynamic topography (Moucha et al., 2008; Rowley et al., 2013; Austermann et al., 2018), and changes in Earth's gravitational field (e.g., Farrell and Clark, 1977; Tamisiea et al., 2001).

Most studies of gravitationally self-consistent sea-level have focused on sea-level responses to changes in the distribution of grounded ice (e.g., Farrell and Clark, 1977; Milne et al., 2001; Mitrovica et al., 2001; Lambeck et al., 2003). Comparatively fewer studies have investigated gravitationally self-consistent sea-level changes due to sediment redistribution (e.g., Dalca et al., 2013; Wolstencroft et al., 2014; Ferrier et al., 2015; Kuchar et al., 2018; Karpytchev et al., 2018). Herein, we use the term "sediment redistribution" to refer to the net effects of erosion and deposition of bedrock and sediment. These studies have shown that sediment deposition can affect inferences of past sea level by several meters on millennial timescales (e.g., Dalca et al., 2013; Ferrier et al., 2015) and tens of meters over Myr timescales (e.g., Moucha and Ruetenik, 2017) by inducing isostatic responses and modifying the gravitational field in an area of up to hundreds of km. Recently, the gravitationally self-consistent sea-level theory has been extended to account for sediment compaction and sediment water storage (Ferrier et al., 2017, 2018).

On passive margins, regional changes in sea level over kyr timescales can be dominated by sediment mass redistribution across the Earth's surface by erosion and deposition, which deform the crust, perturb the gravity field, and shift Earth's rotation axis (e.g., Blum et al., 2008; Wolstencroft et al., 2014; Ferrier et al., 2015;Moucha and Ruetenik, 2017). To date, most studies of gravitationally self-consistent sea-level responses to sediment redistribution have focused on the role of rapid deposition, which in many environments is fastest near the coast, where it generates crustal subsidence and local sea-level rise. Comparatively less work has evaluated the sensitivity of sea-level change to rapid erosion. McGinnis et al. (1993), for example, showed that erosional retreat of continental shelves during lowstands can result in tens of meters of uplift over Myr timescales, which would result in overestimates of sea-level change at the Eocene-Oligocene transition if not properly accounted for. Blum et al. (2008) showed that erosional unloading during lowstands in the Mississippi delta region has resulted in net uplift of the land surface by > 9 m. Similarly, Ruetenik et al. (2019) showed that erosional unloading on a passive margin during lowstands can result in 2-3 meters of isostatic uplift per glacial cycle. Such effects may be even larger in regions where exceptionally rapid erosion occurs close to coastlines. Indeed, these results suggest that if erosion close to a coastline were fast enough, the resulting unloading could counteract the loading and subsidence induced by offshore deposition and result in a local net sea-level fall (e.g., Woo et al., 2017). Thus, near-coastal erosion can induce a sea-level response that is opposite in sign from that produced by sedimentation.

Here, we model sea-level responses to sediment redistribution on the rapidly eroding island of Taiwan, where some of the fastest erosion rates on Earth when compared with global compilation studies, e.g. Portenga and Bierman (2011) of 10+ mm/yr (Dadson et al., 2001) occurs within a few tens of km of the modern shoreline. Our goal is to quantify sea-level responses to exceptionally rapid sediment redistribution, which we illustrate using simulations driven by empirically constrained estimates of erosion and deposition rates in Taiwan and its surroundings. In contrast to previous studies that showed sea-level rise in response to sediment redistribution (on the Mississippi, Indus, and Ganges-Brahmaputra deltas; Wolstencroft et al., 2014; Ferrier et al., 2015; Simms et al., 2013; Kuchar et al., 2018; Karpytchev et al., 2018), our model results show that rapid inland erosion in Taiwan generates a large regional sea-level fall. We use these modeled sea-level responses to revise estimates of tectonically driven rock uplift rates along Taiwan's east coast, similar to recent revisions of tectonically driven rock uplift rates along the Pacific coast of North America (Creveling et al., 2015; Simms et al., 2016).

2. Geologic setting: Taiwan

Taiwan, a product of arc-continent collision, is an island located along the Luzon arc. It is bounded by the Eurasian plate on the northwest and northeast and the Philippine Sea plate to the southeast (Wu, 1978). On the western edge of the island, the Eurasian plate subducts to the east beneath the Philippine Sea plate. The Philippine Sea plate is located in the southeast and subducts beneath the margin of the Eurasian plate northeast of Taiwan along the Ryuku trench (Wu, 1978; Teng et al., 2000). Taiwan is thought to be an archetypical critical wedge in which mass lost by erosion is balanced by shortening and accretion (e.g., Suppe, 1981). Most of the island may be uplifting, but uplift rates may vary spatially (e.g. Fox et al., 2014). Overall Taiwan is moving to the NW and converging against the Chinese continental margin at ~80 mm/yr. However, present-day geodetic measurements show that horizontal velocities on the island vary widely, particularly along the Central Valley fault which separates the Coastal Range from the island's interior to the west (Yu et al., 1997). Previous studies suggested an island-wide mean uplift rate of 5 mm/yr (Suppe, 1989), while more recently it has been suggested that long-term uplift rates may be highest in the north central part of the island, and lower in the south (e.g., Fox et al., 2014). Modern geodetic measurements suggest that the southern Coastal Range may be uplifting at rates ranging from 0 mm/yr on the eastern margin to >10 mm/yr in the western margin (Hsu et al., 2018).

Crustal thickness may be 40 km or higher (Szwillis et al., 2016). Rapid uplift has produced high topography (> 3 km) in the Central Range that is thought to have begun around 4 Ma (Suppe, 1981). Along the central eastern shore, the ~1.5 km high Coastal Range is thought to have uplifted more recently (e.g., Fox et al., 2014; Hsu et al., 2016).

Due to its wet, monsoonal climate and rapid rock uplift rates, Taiwan experiences some of the fastest exhumation and erosion rates on the planet (e.g., Portenga and Bierman, 2011; Milliman and Farnsworth, 2011). Myr-scale exhumation rates reach 6-10 mm/yr (Liu et al., 2001; Willett et al., 2003) and modern decadal-scale, basin-averaged erosion rates are as high as ~12 mm/yr have been reported (Dadson et al., 2003). Offshore postglacial deposition rates exceed 10 mm/yr in the Taiwan Strait (Liu et al., 2008). Ongoing, rapid uplift of the eastern Coastal Range has uplifted and exposed a series of marine deposits along Taiwan’s east coast that formed during the last 15 ka (e.g., Hsieh et al., 2004; Figure 1). The close proximity (< 20 km) of these rapid erosion and deposition rates to dated SL markers make Taiwan an ideal setting to investigate the joint influence of erosion and deposition on sea-level change.

3. Methods

3.1 Model overview

To explore the influence of rapid erosion and deposition on modeled sea-level change, we adopt the methodology of Ferrier et al. (2017), which extended the gravitationally self-consistent sea-level theory of Dalca et al. (2013) by accounting for sediment compaction and sedimentary water storage. Here we give a brief overview of the model and refer the reader to these references for a full description of the model.

Following Farrell and Clark (1976), we compute the change in sea level from one time to another (ΔSL) as the elevation difference between the sea surface and the solid surface (Equation 1). ΔH and ΔI are changes in the thicknesses of sediment and grounded ice, respectively, and ΔG and ΔR are the resulting changes in the elevations of the sea-surface gravitational equipotential and bedrock, respectively. In Equation 1, each of these terms is implicitly a function of time and space.

$$\Delta SL = \Delta G - \Delta H - \Delta I - \Delta R \tag{1}$$

Here, ΔH and ΔI are imposed *a priori* and used to drive the model, while ΔG and ΔR are computed as responses to ΔH and ΔI (Dalca et al., 2013; Ferrier et al., 2017). As in most implementations of the gravitationally self-consistent sea-level theory, we compute ΔG and ΔR using a spherically symmetric Earth model (Kendall et al., 2005; de Boer et al., 2017) following viscoelastic Love number theory (Peltier, 1974; Dalca et al., 2013). These are computed up to spherical harmonic degree and order 1024. The Earth model we adopt is characterized by a viscoelastic mantle with radially varying elasticity and density profiles taken from PREM (Dziewonski and Anderson, 1981), viscosities of the upper and lower mantle of 5×10^{20} Pa s and 5×10^{21} Pa s, respectively (e.g., Austermann et al., 2015), and an effective elastic lithospheric thickness (T_e). To illustrate the influence of T_e on modeled sea-level responses, we present results from two simulations with identical mantle properties but different T_e values. In the first, SL10, we set T_e = 10 km, consistent with estimates for southwestern Taiwan (e.g., Lin and Watts., 2002). In the second, SL30, we set T_e = 30 km, consistent with estimates for central Taiwan (Chen et al., 2013). We apply this range of T_e values because they are consistent with regional estimates of the effective elastic lithospheric thickness, unlike the higher T_e value in the VM2 Earth model, which was used in the inversion for the ICE-5G ice history (Peltier, 2004). Applying an artificially large T_e value would produce an artificially long-wavelength response to the sediment redistribution history in Taiwan, which would mask the spatial variations in sedimentary effects on sea-level change that are the central focus of this study.

In all simulations, we apply a history of ice mass variations ΔI given by ICE-5G (Peltier, 2004), extended from the Last Glacial Maximum to the Last Interglacial (122 ka) following Raymo et al. (2011).

3.2 Sediment redistribution history

The quantities required to model sea-level responses to sediment redistribution are mean sediment porosity $\bar{\phi}$, mean sediment density $\bar{\rho}_H$, and the change in sediment thickness ΔH (Ferrier et al., 2017) These require knowledge of the rates and patterns of erosion and deposition across the study region throughout the time period of interest.

We constructed maps of erosion and deposition rates to drive model sea-level responses (Figure 2). To construct the history of erosion on land, we applied the average erosion rates for Taiwan over the past ~80 ka inferred from inverse stream profile modeling (Fox et al., 2014). In our simulations these rates vary in space and are constant in time as the 120-kyr duration of our simulations is similar to the ~80-kyr timestep used by Fox et al. (2014). Erosion rates are highest in the Central Range, reaching up to 12 mm/yr, and gradually drop to nearly 0 mm/yr near the Western Foothills near the coastal plain. Our sediment redistribution history is characterized by sediment deposition that is thickest on the eastern margin where there is greater accommodation, while sedimentary deposits are thinner and more widely dispersed along the shallow western margin. Modeled deposition rates and patterns evolve over time, such that during highstands deposition is concentrated near the shore on the shallow west coast, while during lowstands, depocenters on the west coast move outboard. On the east coast deposited sediment slowly progrades outboard but the depocenter locations and deposition rates remain relatively constant in space and time.

To reconstruct the history of deposition, we adopted published measurements of Holocene deposition rates on Taiwan's western coastal plain and the Taiwan Strait, inferred from measurements of post-glacial sediment thickness (Liu et al., 2008). In the absence of measurements of higher-frequency deposition rate variations, we apply these as temporally steady deposition rates from 12 ka to the present in these regions. As far as we are aware, there are few empirical constraints on deposition rates for periods further in the past and at other locations offshore around Taiwan. For these periods and regions, we use the fluvial land-to-ocean sediment fluxes determined from upstream integration of erosion by Fox et al. (2014) to drive a geometric sediment deposition model (Reynolds et al., 1991; Ruetenik et al., 2016), which computes the growth of sedimentary deposits at the outlets of Taiwan's major rivers. In this model, sediment transport from source (land) to sink (nearest ocean outlet) is assumed to be instantaneous. This deposition model distributes sediment in a conical shape, such that if the sediment source (river outlet) remained stationary over time, the plan view morphology of the deposit would be shaped like a wedge of a circle, with a point at the river outlet, two straight sides emanating seaward from that point, and an arc segment connecting the sides. In profile, the deposit slopes downward at a constant "cone angle" from the high point at the river outlet to the ocean floor. If the model sedimentary deposit fills up (aggrades) to sea level, then the deposit progrades at a constant "subaerial angle". We take the cone angle to be 1°, consistent with the present-day angle of the continental slope on the southern edge of Taiwan (further away from the Ryuku trench), and 0.02° for the "subaerial angle", consistent with the shelf slope on the western margin. In this construction, the location of the cone's source point varies over time as the shoreline migrates, which we compute in a sea-level simulation driven by ice mass variations at 1-kyr timesteps. The deposition model adopts a DEM with present-day bathymetry at ~900 m resolution (SRTM30+, Becker et al., 2007), and modeled deposition patterns evolve according to the spatial variations in bathymetry throughout the model run.

Because the modeled deposits are fed by the eroded mass fluxes from 122 to 12 ka, over this time period the integrated eroded mass over the model domain equals the integrated deposited mass. From 12 ka to the present, modeled deposition rates in the Taiwan Strait increase from zero (Figure 2b) to the values adopted from Liu et al. (2008) (Figure 2c), which results in an integrated deposition rate that is ~1.4 times higher than the integrated erosion rate during this time. The temporal evolution of bathymetry is part of the reason why sediment deposition patterns are different in the previous highstand (Figure 2a) relative to those in the present highstand (Figure 2c).

Since this 12-kyr duration is ~10% of the 122-kyr simulation, over the duration of the simulation the cumulative deposited mass is ~4% higher than the cumulative eroded mass.

For depositional areas, we follow Ferrier et al. (2017, 2018) in computing the rate of change of sediment thickness as the difference between the rates of deposition and compaction, with sediment deposited at an initial porosity of 0.6 and compacting at a rate given by Equation 2.

$$\frac{d\phi(z)}{dt} = -k\sigma_d(z)(\phi(z) - \phi_{min}) \quad (2)$$

Here $\phi(z)$ is the porosity at depth z below the sediment surface, ϕ_{min} is the minimum porosity in fully compacted sediment, k is a compaction coefficient, and $\sigma_d(z)$ is the difference between lithostatic and hydrostatic stress at depth z, which depends on the sediment grain density ρ_s and water density ρ_w. Following Ferrier et al. (2017, 2018), we adopt values of ρ_s = 2700 kg m^{-3}, ρ_w = 1000 kg m^{-3}, ϕ_{min} = 0.2, and $k = 10^{-17}$ Pa^{-1} s^{-1}. This approach yields vertical profiles of sediment density and porosity that vary over time, which we use to compute time series of mean sediment column density $\bar{\rho}_H$, mean sediment column porosity $\bar{\phi}$, and sediment thickness ΔH throughout the depositional region. These are the sedimentary inputs with which we drive the sea-level simulations.

4. Results

We used the model in Section 3 to compute sea-level changes over the last glacial cycle (122 ka) in two simulations, one driven by sediment redistribution and global ice volume change, and the other driven only by global ice volume change (Figure 3). In each simulation, the Earth model has the same effective elastic lithospheric thickness T_e = 30 km, consistent with estimates for central Taiwan (Chen et al., 2013). The difference between these simulations is shown in the right-hand column in Figure 3, which reveals the net effect of sediment redistribution on sea-level change.

The combination of the responses in crustal elevation and sea-surface equipotential yield the response in sea level. Figure 3a shows the sea-level response as $\Delta SL_{GR} = \Delta G - \Delta R$, which is the relevant quantity to compare to sea-level changes inferred from paleo-sea-level markers, since such markers have avoided direct changes in ice thickness and sediment thickness and, thus, locally have $\Delta I = 0$ m and $\Delta H = 0$ m in Equation 1 (e.g., Ferrier et al., 2017). Here, the pattern of high ΔSL_{GR} is dominated by the response in ΔR, as is common in responses to sediment redistribution (e.g., Dalca et al., 2013; Wolstencroft et al., 2014; Ferrier et al., 2015).

The dominant response to erosion is a dome-like pattern of rock uplift (i.e., positive ΔR) which reaches a maximum amplitude of 170 m in central Taiwan (Figure 3b). This response in ΔR has a wavelength of ~300-500 km, dropping off to 5% of its maximum amplitude at distances of ~150-250 km from the dome center. By comparison, the response of the sea-surface equipotential, ΔG, to sediment redistribution is smaller, with a maximum amplitude of 6 m (Figure 3c).

To illustrate the sensitivity of the modeled responses to the effective elastic thickness, we conducted a second simulation with the same ice and sediment redistribution histories as in Figure 3, but with a lithospheric effective elastic thickness of 10 km instead of 30 km. A comparison of these results show that the adopted effective elastic thickness affects both the wavelength and amplitude of the modeled sea-level responses (Figure 4). The maximum amplitude of the sea-level response is larger in the simulation with the less rigid lithosphere (SL10), reaching 370 m (compared with 170 m in the simulation with the more rigid lithosphere, SL30). These sea-level responses are large mainly because the subaerial eroded thickness is large, totaling >600 m in the most rapidly eroding areas over the 122-kyr simulation. In contrast, the lateral extent of the response, which we operationally define as the distance from the location of maximum ΔSL to the nearest point where ΔSL drops to 5% of the maximum response, is larger in the simulation with more rigid lithosphere, approximately 65 km in SL10 and 145 km in SL30.

5. Discussion

5.1 Patterns and drivers of modeled sea-level change

Figure 4 shows that modeled sea-level responses to sediment redistribution form a bulls-eye pattern around Taiwan with a radius that depends on the lithosphere's effective elastic thickness. Along Taiwan's east coast, sediment loading over the 122-kyr simulation induced a sea-level fall of 120-138 m in the 30-km T_e simulation and 113-180 m in the 10-km T_e simulation (Figure 4). This largely reflects crustal uplift (ΔR) in response to erosional unloading on land since the crustal response is much larger than the gravitational response (ΔG; Figure 3), consistent with previous studies (e.g., Dalca et al., 2013). This behavior, in which sediment redistribution drives sea-level fall rather than sea-level rise, is unusual relative to many coastal sites with large sediment fluxes elsewhere around the world. In many large river systems, the area on both sides of the coast is dominated by sediment deposition, both in marine deposits offshore and in low-gradient floodplains on land (e.g., the Mississippi, Indus, and Yellow River deltas; Wolstencroft et al., 2014; Ferrier et al., 2015; Pico et al., 2016; Kuchar et al., 2018). In such areas, the combination of subaerial and submarine deposition induces a broad region of crustal subsidence both onshore and offshore, which in turn drives sea-level rise along the coast.

Meanwhile, the eastern side of Taiwan is characterized by rapid erosion on land and rapid deposition offshore (Figure 2). As Figure 3a shows, the crustal uplift induced by erosion more than offsets the subsidence induced by deposition offshore, such that the coast experiences net uplift and hence sea-level fall. This is due in part to the fact that the change in the total load is larger for a given mass of subaerial eroded sediment than for the same mass of submarine deposited sediment. The space occupied by newly deposited marine sediment had formerly been occupied by water, whereas the space evacuated by eroded subaerial sediment is replaced by air. The magnitude of the total mass load change is therefore greater for a given mass of eroded sediment than for the same mass of deposited marine sediment. The magnitude of the sea-level fall is large relative to estimates of changes in global mean sea level from the Last Interglacial to the present (6-9 m; Kopp et al., 2009; Dutton and Lambeck, 2012). This illustrates that erosion near coasts can strongly affect both the magnitude and the sign of present-day paleoshoreline and SL marker elevations.

5.2 Comparison of modeled sea-level changes to observed sea-level changes

In many coastal regions around the world, the most prominent SL markers and paleoshorelines are those that formed during the Last Interglacial (LIG). These are often well preserved because the combined effects of eustatic, crustal, and gravitational changes since the LIG tend to leave them a relatively short vertical distance above the modern sea surface and relatively free of erosional modification (e.g., Merritts and Bull, 1989; Dutton and Lambeck, 2012; Creveling et al., 2015, 2017). In eastern Taiwan, however, our simulations suggest that LIG SL markers should lie at much higher elevations, with sediment redistribution alone generating 80-150 m of rock uplift relative to the modern sea surface. More problematically for sea-level reconstructions, the same intense erosional processes that induce rapid uplift of Taiwan's sea-level markers also induce their rapid destruction. As a result, no preserved LIG sea-level markers are reported from eastern Taiwan, as far as we are aware. Instead, the oldest known sea-level markers in this region are no older than ~15 ka (Hsieh et al, 2004). Thus, our ability to compare modeled sea-level changes to observed sea-level changes in Taiwan stretches back no further than the past 15 kyr.

RSL markers vary by type, from fossils to anthropogenic artifacts, and each type has an associated, and often broad, indicative range of paleo water depth (Rovere et al., 2016). The RSL data presented in Hsieh et al. (2004) contains a range of well-constrained sea-level markers (deposited within one meter of sea level), as well as markers which have an unconstrained range of deposition. These consist of fossil wood, peat, shells, algae, and corals. As in Hsieh et al. (2004), we assume that tectonic uplift rates based on the unconstrained RSL markers are minima. For a rigorous discussion of RSL marker depth uncertainty we refer the interested reader to Hsieh et al. (2004). Here we adopt these bounds in assessing the influence of sediment redistribution on inferred tectonic uplift rate.

In Figure 5, local sea-level histories inferred from dated sea-level markers are shown as gray boxes and triangles, the sizes of which indicate uncertainties in SL marker elevation and age (Hsieh et al., 2004). Triangles represent unconstrained deposits that provide only a lower bound on elevation. Since the ~4-15 ka ages of these paleo-sea-level markers are much older than the ~10^2-year duration of the earthquake cycle (Chen, 2003), they reflect the cumulative change in sea level due to the combination of tectonic deformation (coseismic inelastic strain and interseismic elastic strain) and the responses to sediment redistribution and ice mass changes.

Superimposed on the data are modeled relative sea level histories, $RSL(t)$, that represent the difference between sea level at a past time t and the present time t_p. This is defined as $RSL(t) = SL_{GR}(t) - SL_{GR}(t_p)$, which is equivalent to $-\Delta SL_{GR}$ from t to t_p (e.g., Ferrier et al., 2015). Four modeled sea-level histories are shown in Figure 5, each representing a different combination of loading histories and Earth model. The vertical width of each colored region represents the spatial variability in $RSL(t)$ responses along Taiwan's east coast.

Figure 5 shows that the observed SL markers on Taiwan's east coast sit at higher elevations than the modeled correlative paleo-sea-levels in all simulations. We interpret the differences between modeled and measured elevations as a reflection of tectonically driven rock uplift which are generally smaller in simulations that include the effects of sediment redistribution. Therefore, we suggest that sediment redistribution plays a significant role in explaining the present elevation of Taiwan's sea-level markers. Specifically, the effects of sediment redistribution account for 16-100% of the estimated difference between observed and modeled sea-level marker elevations over the past 10 ka. This implies that sea-level simulations that include sediment redistribution can be used to refine estimates of tectonically driven rock uplift rates inferred from SL markers in Taiwan (see section 5.3).

Our simulations also show that sediment redistribution may have induced significant perturbations in sea level tens of km east of Taiwan. In Figure 6, solid and dashed lines show modeled sea-level changes on the islands of Lutao and Lanyu, ~30-65 km from Taiwan's east coast (Figure 1; Vita-Finzi, 2000; Wang and Burnett (1990)). At each of these sites, the role of sediment redistribution in *RSL* change is small relative to those in eastern Taiwan. On Lutao and Lanyu, however, the responses are large enough to be significant relative to the elevation of SL markers there. For example, sediment redistribution perturbs modeled *RSL* estimates in Lutao by up to 4 meters at 6 ka, which is greater than the 1-3 m elevation of the 4-6 ka correlative SL marker elevation there (Vita-Finzi, 2000; Wang and Burnett (1990)).

All sea-level markers are subject to uncertainty in age and depth of deposition. The depth of deposition reported in Hsieh et al. (2004) ranges from -1 to 1 meters for some markers (negative values indicating deposition on land by tidal processes) and upwards of 10 meters for others (Supplementary Table 1). For other data sets, depth ranges were not reported (Wang and Burnett, 1990; Vita-Finzi, 2000), in part because the species of corals were not reported for some markers, and corals can range in depth from 3 to 20 m (Wang and Burnett, 1990). We therefore consider estimates of rock uplift based on these sea-level markers to be lower bounds.

5.3 Influence of sediment redistribution on inferences of tectonically driven uplift

The influence of sediment redistribution on sea level has important implications for efforts to use paleo-sea-level changes to infer tectonically driven rock uplift rates. These are often determined by rewriting Equation 1 as $\Delta R = \Delta G - \Delta SL = \Delta G + RSL$ (e.g., Muhs et al., 1990; Creveling et al., 2015; Simms et al., 2015) and attributing ΔR to tectonically driven rock uplift. In practice, RSL is often determined from the elevations and ages of paleo-sea-level markers, while ΔG is often determined from simulations of sea-level change driven by global ice changes. Tectonically driven rock uplift rates are then calculated as $U_{\text{tectonic}} = \Delta R/\Delta t$, where Δt is the age of the paleo-sea-level marker.

In places like Taiwan that experience significant sediment redistribution, a portion of ΔR is generated by isostatic responses to surface loads. Therefore, only a fraction of ΔR is attributable to tectonically driven rock uplift. In such places, we may write $\Delta R \approx \Delta R_{\text{sediment}}$ +

$\Delta R_{tectonic}$, where $\Delta R_{sediment}$ is the sediment-driven change in crustal elevation and $\Delta R_{tectonic}$ is the residual change in crustal elevation by tectonically driven rock uplift. This approximation is appropriate to the extent that other contributions to vertical crustal motion (e.g., by dynamic topography) are small relative to those driven by sediment and tectonics. A global simulation of sea-level responses to dynamic topography suggest a rate of sea-level change of 0.04 mm/yr driven by dynamic topography off Taiwan's east coast over the past glacial cycle (Austermann et al., 2017), which is <1% of the maximum rates of vertical motion inferred for our study sites in Taiwan (Figure 6). We therefore suggest that contributions to ΔR from dynamic topography are likely to be small relative to the contributions from sediment and tectonics in Taiwan, and that $\Delta R \approx \Delta R_{sediment} + \Delta R_{tectonic}$ is a reasonable approximation for our study sites. Under this approximation, revised estimates of tectonically driven rock uplift rates can be calculated as $U_{tectonic} = \Delta R_{tectonic}/\Delta t = (\Delta R - \Delta R_{sediment})/\Delta t$.

We calculate $\Delta R_{tectonic}$ as the difference between observed *RSL* and modeled *RSL*, where the former is determined from SL marker elevations (which yield ΔR), and the latter is determined from simulations driven by regional sediment redistribution and global ice changes (which yield $\Delta R_{sediment}$; e.g., Figure 3a). The observations and simulations are summarized in Figure 5, which shows observed SL marker ages and elevations along Taiwan's east coast (black boxes and triangles) as well as modeled *RSL* histories in the same region in simulations driven by sediment and ice variations or only by ice variations.

Figure 5 reveals that sediment redistribution in Taiwan has significant effects on modeled *RSL* histories and hence estimates of $\Delta R_{tectonic}$. For example, at 10 ka, modeled *RSL* is ~3.9 ± 6.5 m in simulations that include sediment redistribution and -10.9 ± 1.4 m in simulations that neglect it. Thus, accounting for sediment redistribution can reduce estimates of $\Delta R_{tectonic}$ by

~14.8 ± 6.6 m at 10 ka along Taiwan's east coast. For the lower-altitude SL markers at 10 ka, which presently have an elevation of ~14 m, this reduces estimates of $\Delta R_{\text{tectonic}}$ by more than a factor of 2, from 24.9 ± 1.4 m (14 m – (-10.9 ± 1.4 m)) to 10.1 ± 6.5 m (14 m – (3.9 ± 6.5 m)) (Figure 5).

We use these revised estimates of $\Delta R_{\text{tectonic}}$ to calculate new estimates of tectonically driven rock uplift rates. At each area along Taiwan's east coast (correlative regions as defined by Hsieh et al., 2004), we calculate U_{tectonic} (Figure 7a) as the slope of a linear regression between $\Delta R_{\text{tectonic}}$ and SL marker age forced through the origin (Figure 7b), since both observed and modeled *RSL* must be zero at present. To demonstrate the effects of sediment redistribution on estimates of U_{tectonic}, we calculate what the inferred tectonically driven rock uplift rates would have been if sediment redistribution were neglected. We term this $U_{\text{tectonic, ice-only}}$, and we calculate it as the rate of change of $\Delta R_{\text{tectonic, ice-only}}$, which is the difference between the observed *RSL* and modeled *RSL* in a simulation driven only by ice changes (Figure 3d). As with U_{tectonic}, we calculate $U_{\text{tectonic, ice-only}}$ as the slope of a linear regression between $\Delta R_{\text{tectonic, ice-only}}$ and SL marker age.

Figure 7 shows these revised estimates of U_{tectonic}, which reveal that sediment redistribution can have a significant effect on estimates of tectonically driven rock uplift rates. Estimates of U_{tectonic} are ~1-2 mm yr^{-1} lower than $U_{\text{tectonic, ice-only}}$, which vary with latitude from ~0 to 6 mm yr^{-1}. This implies that estimates of tectonically driven uplift rates inferred from SL markers along Taiwan's coast would be significantly reduced by accounting for the effects of sediment redistribution on sea-level change. The patterns of uplift remain unchanged, with uplift rates generally tapering off near the inferred fault at 23°N (e.g., Vita-Finzi and Lin, 1998; Figure 7).

Lastly, our revised estimates of U_{tectonic} show that accounting for sediment redistribution can help refine the magnitude of inferred rock uplift rates across spatial discontinuities in rock uplift rate. In Figure 7a, inferred rock uplift rates reach a minimum of about -1.5 mm/yr in the T_e = 30 km Earth model at ~23°N, which is the location of a proposed fault (Vita-Finzi and Lin, 1998). These rates increase to near their maximum rates just south of this fault, and gradually increase to the north to ~5 mm/yr before decreasing again around 23.3°N. Around 23.5°N rates reach a local minimum of at least ~0 mm/yr before increasing again to a local maximum of ~5 mm/yr at 23.7°N. This discontinuity in rock uplift rate is apparent in simulations driven by ice and sediment, as well as in simulations driven only by ice mass variations. These short-wavelength (tens of km) variations are unlikely to be driven by sediment redistribution, which in these simulations drives sea-level changes that vary smoothly over wavelengths >100 km (Figure 3). Our revised rock uplift rates are therefore consistent with the interpreted location of the proposed fault.

5.4 Sensitivity to sediment redistribution history and Earth model

Uncertainties in modeled sea-level responses depend on the uncertainties in several factors, including the reconstructed sediment redistribution history, the adopted Earth model, and, to a lesser extent in our study area, the adopted global ice history. Uncertainties associated with the ice history are comparatively small because the ΔSL response to ΔI in Taiwan is much smaller than the response to ΔH (e.g., compare Figures 3a and 3d). This is a consequence of the >8000-km distance between Taiwan and the Antarctic, Laurentide and Fennoscandian ice sheets, which were the main locations of ice mass variations over the last glacial cycle. Thus, here we focus on the uncertainties in the sediment redistribution history and the Earth model.

Our reconstruction of the sediment redistribution history has uncertainties that vary in space and time, partly because some sites have more erosion and deposition rate measurements than others, and partly because empirical constraints on erosion and deposition rates are rarer deeper in the past. Modeled erosion rates have uncertainties up to a factor of 2 related to the time-space relationship used in the stream profile inversions (Fox et al., 2014). Additionally, we are unaware of deposition rate measurements that predate the Holocene on the west coast and of any age on the east coast. For areas lacking deposition rate measurements, the applied deposition rates and patterns depend on the deposition model parameters (cone and shelf angle). Thus, for some regions and time periods, empirical data are unable to provide strong constraints on past variations of sediment redistribution.

However, other aspects of the sediment redistribution history are relatively well constrained. The highest erosion rates in the predicted sediment redistribution history (~12 mm/yr) are consistent with previously published estimates of highest channel incision rates (Dadson et al., 2003) of 9 to >15 mm/yr. Similarly, the fastest deposition rates in our sediment redistribution history (152 mm/yr distributed over a 400-km^2 region, mass load 66 Mt/yr) are broadly consistent with fluvial sediment fluxes as high as 88 Mt/yr out of the east coast rivers feeding these deposits (Dadson et al., 2003). The total island-wide eroded sediment discharge 192 Mt/yr is only ~7% higher than the 20-year average sediment discharge reported by Kao and Milliman (2008) of 180 Mt/yr transported by the 16 largest rivers. Given that sea-level responses are approximately linearly related to the cumulative sediment flux for a given sediment redistribution geometry (Ferrier et al., 2015, 2017), this suggests that uncertainties associated with the total sediment flux may be relatively small in these simulations.

Modeled sea-level changes are also sensitive to the choice of Earth model. For example, Figures 5 and 6 reveal significant differences in sea-level responses between the SL30 and SL10 simulations, which differ only in the effective elastic thickness of the lithosphere (30 km and 10 km, respectively). In the SL10 simulations, marine deposition induces crustal subsidence with a larger amplitude and shorter wavelength than in the SL30 simulations, because crustal responses are flexurally filtered more strongly by the more rigid lithosphere in the SL30 simulations. These effects are especially apparent on the island of Lanyu, where RSL_{GR} at 8 ka is as much as 8 meters higher in SL30 simulations than in SL10 simulations (Figure 6). As a result, ΔSL_{GR} in Lanyu and Lutao increases in the SL10 simulations and decreases in the SL30 simulations, highlighting the sensitivity of modeled sea-level responses to T_e. As stated in Section 5.2, we consider estimates of rock uplift to be lower bounds for those sites based on sea-level markers without reported lower bounds on the depth of formation.

Lastly, we note that sea-level responses in our simulations are governed by a spherically symmetric Earth model, a characteristic shared by nearly all implementations of the sea-level theory due to the computational expense of computing sea-level responses with a laterally varying 3-D Earth model (e.g., Latychev et al., 2005; de Boer et al., 2017; Gomez et al., 2018; Crawford et al., 2018). This approach necessarily neglects several things that may affect sea-level changes in Taiwan, including lateral variations in mantle and lithospheric properties (viscosity, elasticity, density, thickness), brittle crustal deformation, and crustal underplating, and other tectonic processes (e.g., Suppe, 1984). Like all other spherically symmetric implementations of the sea-level model, our simulations cannot account for these processes, so we emphasize that our modeled sea-level responses isolate the sea-level change driven by sediment redistribution, which is a portion of the total sea-level change. Nonetheless, our simulations illustrate the sensitivity of sea-level responses to Earth model characteristics, and they motivate ongoing efforts to constrain regional variations in these characteristics. and to develop methodologies that can account for them.

6. Conclusions

The central contribution of this study is new simulations showing that the combination of rapid onshore erosion and rapid offshore deposition is capable of generating rapid sea-level fall along Taiwan's east coast. Our simulations imply that sediment redistribution is large enough to have driven sea-level fall along Taiwan's eastern shore of >10 m over the past 10 ka and >100 m since the last interglacial at ~120 ka. Contrary to the behavior observed in many other coastal areas with massive sediment fluxes (e.g., large deltas), sediment redistribution around Taiwan tends to drive sea-level fall, rather than sea-level rise.

The sediment-driven sea-level fall can help resolve elevation differences between observed paleo-sea-level markers in Taiwan and modeled sea-level changes, and our simulations imply that sediment redistribution may have affected SL marker elevations on islands as far away as ~100 km from Taiwan. This suggests that a significant portion of recent crustal uplift along Taiwan's east coast may be caused in part by erosional unloading, which in turn suggests that estimates of tectonically driven rock uplift rates inferred from paleo-sea-level markers may need to be revised downward by as much as 2 mm/yr in this region. These results highlight the importance of accounting for sediment redistribution—particularly rapid erosion—in interpretations of past sea-level change in tectonically active regions.

Acknowledgments

GAR and KLF were supported by NASA award 16-IDS16-0093, and KLF was supported by ACS-PRF award 58209-DNI8 and NSF award EAR-1525922. MF was supported by NERC award NE/N015479/1. We thank Jacqueline Austermann for providing sea level code, Robert Moucha for helpful discussion, and two anonymous reviewers whose comments greatly improved the manuscript.

References

Austermann, J., Mitrovica, J. X., Latychev, K., & Milne, G. A. (2013). Barbados-based estimate of ice volume at Last Glacial Maximum affected by subducted plate. Nature Geoscience, 6(7), 553.

Austermann, J. and Mitrovica, J.X., 2015. Calculating gravitationally self-consistent sea level changes driven by dynamic topography. *Geophysical Journal International*, *203*(3), pp.1909-1922.

Austermann, J., Mitrovica, J.X., Huybers, P. and Rovere, A., 2017. Detection of a dynamic topography signal in last interglacial sea-level records. *Science Advances*, *3*(7), p.e1700457.

Becker, J. J., D. T. Sandwell, W. H. F. Smith, J. Braud, B. Binder, J. Depner, D. Fabre, J. Factor, S. Ingalls, S-H. Kim, R. Ladner, K. Marks, S. Nelson, A. Pharaoh, R. Trimmer, J. Von Rosenberg, G. Wallace, P. Weatherall., Global Bathymetry and Elevation Data at 30 Arc Seconds Resolution: SRTM30_PLUS, Marine Geodesy, 32:4, 355-371, 2009.

Chen, B., Chen, C., Kaban, M.K., Du, J., Liang, Q. and Thomas, M., 2013. Variations of the effective elastic thickness over China and surroundings and their relation to the lithosphere dynamics. *Earth and Planetary Science Letters*, *363*, pp.61-72.

Chen C., 2003. Accelerating seismicity of moderate-size earthquakes before the 1999 Chi-Chi, Taiwan, earthquake: Testing time-prediction of the self-organizing spinodal model of earthquakes, Geophysical Journal International, Volume 155, Issue 1, Pages F1–F5, https://doi.org/10.1046/j.1365-246X.2003.02071.x

Chen, Y.W., Shyu, J.B.H. and Chang, C.P., 2015. Neotectonic characteristics along the eastern flank of the Central Range in the active Taiwan orogen inferred from fluvial channel morphology. *Tectonics*, *34*(10), pp.2249-2270.

Crawford, O., Al-Attar, D., Tromp, J., Mitrovica, J. X., Austermann, J., & Lau, H. C. (2018). Quantifying the sensitivity of post-glacial sea level change to laterally varying viscosity. Geophysical journal international, 214(2), 1324-1363.

Creveling, J.R., Mitrovica, J.X., Hay, C.C., Austermann, J. and Kopp, R.E., 2015. Revisiting tectonic corrections applied to Pleistocene sea-level highstands. *Quaternary Science Reviews*, *111*, pp.72-80.

Creveling, J. R., Mitrovica, J. X., Clark, P. U., Waelbroeck, C., & Pico, T. (2017). Predicted bounds on peak global mean sea level during marine isotope stages 5a and 5c. Quaternary Science Reviews, 163, 193-208.

Dadson, S.J., Hovius, N., Chen, H., Dade, W.B., Hsieh, M.L., Willett, S.D., Hu, J.C., Horng, M.J., Chen, M.C., Stark, C.P. and Lague, D., 2003. Links between erosion, runoff variability and seismicity in the Taiwan orogen. *Nature*, *426*(6967), p.648.

Dalca, A.V., Ferrier, K.L., Mitrovica, J.X., Perron, J.T., Milne, G.A. and Creveling, J.R., 2013. On postglacial sea level—III. Incorporating sediment redistribution. *Geophysical Journal International*, *194*(1), pp.45-60.

de Boer, B., Stocchi, P., Whitehouse, P.L. and van de Wal, R.S., 2017. Current state and future perspectives on coupled ice-sheet–sea-level modelling. *Quaternary Science Reviews*, *169*, pp.13-28.

Doar, W.R. and Kendall, C.G.S.C., 2014. An analysis and comparison of observed Pleistocene South Carolina (USA) shoreline elevations with predicted elevations derived from Marine Oxygen Isotope Stages. *Quaternary Research*, *82*(1), pp.164-174.

Dutton, A., & Lambeck, K. (2012). Ice volume and sea level during the last interglacial. Science, 337(6091), 216-219.

Dziewonski, A.M. and Anderson, D.L., 1981. Preliminary reference Earth model. *Physics of the earth and planetary interiors*, *25*(4), pp.297-356.

Farrell, W. E., & Clark, J. A. (1976). On postglacial sea level. Geophysical Journal of the Royal Astronomical Society, 46(3), 647-667.

Ferrier, K.L., Mitrovica, J.X., Giosan, L. and Clift, P.D., 2015. Sea-level responses to erosion and deposition of sediment in the Indus River basin and the Arabian Sea. *Earth and Planetary Science Letters*, *416*, pp.12-20.

Ferrier, K.L., Austermann, J., Mitrovica, J.X. and Pico, T., 2017. Incorporating sediment compaction into a gravitationally self-consistent model for ice age sea-level change. *Geophysical Journal International*, *211*(1), pp.663-672.

Ferrier, K. L., Li, Q., Pico, T., & Austermann, J. (2018). The Influence of Water Storage in Marine Sediment on Sea-Level Change. Geophysical Research Letters, 45(5), 2444-2454.

Fox, M., Goren, L., May, D.A. and Willett, S.D., 2014. Inversion of fluvial channels for paleorock uplift rates in Taiwan. *Journal of Geophysical Research: Earth Surface*, *119*(9), pp.1853-1875.

Gomez, N., Latychev, K. and Pollard, D., 2018. A Coupled Ice Sheet–Sea Level Model Incorporating 3D Earth Structure: Variations in Antarctica during the Last Deglacial Retreat. *Journal of Climate*, *31*(10), pp.4041-4054.

Haskell, N. A. (1935). The motion of a viscous fluid under a surface load. Physics, 6(8), 265-269.

Hsu, W.H., Byrne, T.B., Ouimet, W., Lee, Y.H., Chen, Y.G., Soest, M.V. and Hodges, K., 2016. Pleistocene onset of rapid, punctuated exhumation in the eastern Central Range of the Taiwan orogenic belt. *Geology*, *44*(9), pp.719-722.

Hsu, Y.J., Lai, Y.R., You, R.J., Chen, H.Y., Teng, L.S., Tsai, Y.C., Tang, C.H. and Su, H.H., 2018. Detecting rock uplift across southern Taiwan mountain belt by integrated GPS and leveling data. *Tectonophysics*, *744*, pp.275-284.

Hsieh, M.L., Liew, P.M. and Hsu, M.Y., 2004. Holocene tectonic uplift on the Hua-tung coast, eastern Taiwan. *Quaternary International*, *115*, pp.47-70.

Huang, M.H., Hu, J.C., Ching, K.E., Rau, R.J., Hsieh, C.S., Pathier, E., Fruneau, B. and Deffontaines, B., 2009. Active deformation of Tainan tableland of southwestern Taiwan based on geodetic measurements and SAR interferometry. *Tectonophysics*, *466*(3-4), pp.322-334.

Karpytchev, M., Ballu, V., Krien, Y., Becker, M., Goodbred, S., Spada, G., ... & Khan, Z. (2018). Contributions of a Strengthened Early Holocene Monsoon and Sediment Loading to Present-Day Subsidence of the Ganges-Brahmaputra Delta. Geophysical Research Letters, 45(3), 1433-1442.

Kendall, R.A., Mitrovica, J.X. and Milne, G.A., 2005. On post-glacial sea level–II. Numerical formulation and comparative results on spherically symmetric models. *Geophysical Journal International*, *161*(3), pp.679-706.

Kopp, R. E., Simons, F. J., Mitrovica, J. X., Maloof, A. C., & Oppenheimer, M. (2009). Probabilistic assessment of sea level during the last interglacial stage. Nature, 462(7275), 863.

Kuchar, J., Milne, G., Wolstencroft, M., Love, R., Tarasov, L., & Hijma, M. (2018). The influence of sediment isostatic adjustment on sea level change and land motion along the US Gulf Coast. Journal of Geophysical Research: Solid Earth, 123(1), 780-796.

Lambeck, K., Purcell, A., Johnston, P., Nakada, M. and Yokoyama, Y., 2003. Water-load definition in the glacio-hydro-isostatic sea-level equation. *Quaternary Science Reviews*, *22*(2-4), pp.309-318.

Latychev, K., Mitrovica, J. X., Tromp, J., Tamisiea, M. E., Komatitsch, D., & Christara, C. C. (2005). Glacial isostatic adjustment on 3-D Earth models: a finite-volume formulation. Geophysical Journal International, 161(2), 421-444.

Lee, J.C., Chu, H.T., Angelier, J., Chan, Y.C., Hu, J.C., Lu, C.Y. and Rau, R.J., 2002. Geometry and structure of northern surface ruptures of the 1999 Mw= 7.6 Chi-Chi Taiwan earthquake:

influence from inherited fold belt structures. *Journal of Structural Geology*, *24*(1), pp.173-192.

Lin, A.T. and Watts, A.B., 2002. Origin of the West Taiwan basin by orogenic loading and flexure of a rifted continental margin. *Journal of Geophysical Research: Solid Earth*, *107*(B9), pp.ETG-2.

Liu, T.K., Hsieh, S., Chen, Y.G. and Chen, W.S., 2001. Thermo-kinematic evolution of the Taiwan oblique-collision mountain belt as revealed by zircon fission track dating. *Earth and Planetary Science Letters*, *186*(1), pp.45-56.

Liu, J.P., Liu, C.S., Xu, K.H., Milliman, J.D., Chiu, J.K., Kao, S.J. and Lin, S.W., 2008. Flux and fate of small mountainous rivers derived sediments into the Taiwan Strait. *Marine Geology*, *256*(1-4), pp.65-76.

Lisiecki, L.E. and Raymo, M.E., 2005. A Pliocene-Pleistocene stack of 57 globally distributed benthic δ18O records. *Paleoceanography*, *20*(1).

McGinnis, J.P., Driscoll, N.W., Karner, G.D., Brumbaugh, W.D. and Cameron, N., 1993. Flexural response of passive margins to deep-sea erosion and slope retreat: implications for relative sea-level change. *Geology*, *21*(10), pp.893-896.

Merritts, D., & Bull, W. B. (1989). Interpreting Quaternary uplift rates at the Mendocino triple junction, northern California, from uplifted marine terraces. Geology, 17(11), 1020-1024.

Milliman, J. D., & Farnsworth, K. L. (2013). River discharge to the coastal ocean: a global synthesis. Cambridge University Press.

Milne, G.A., Davis, J.L., Mitrovica, J.X., Scherneck, H.G., Johansson, J.M., Vermeer, M. and Koivula, H., 2001. Space-geodetic constraints on glacial isostatic adjustment in Fennoscandia. *Science*, *291*(5512), pp.2381-2385.

Mitrovica, J.X., Tamisiea, M.E., Davis, J.L. and Milne, G.A., 2001. Recent mass balance of polar ice sheets inferred from patterns of global sea-level change. *Nature*, *409*(6823), p.1026.

Moucha, R., Forte, A.M., Mitrovica, J.X., Rowley, D.B., Quéré, S., Simmons, N.A. and Grand, S.P., 2008. Dynamic topography and long-term sea-level variations: There is no such thing as a stable continental platform. *Earth and Planetary Science Letters*, *271*(1-4), pp.101-108.

Moucha, R. and Ruetenik, G.A., 2017. Interplay between dynamic topography and flexure along the US Atlantic passive margin: Insights from landscape evolution modeling. *Global and Planetary Change*, *149*, pp.72-78.

Ruetenik, G., Moucha, R. and de Boer, B., 2019. Deformation in response to landscape evolution during glacial cycles on the US Atlantic passive margin. *Earth and Planetary Science Letters*, *526*, p.115759.

Muhs, D.R., Kelsey, H.M., Miller, G.H., Kennedy, G.L., Whelan, J.F. and McInelly, G.W., 1990. Age estimates and uplift rates for late Pleistocene marine terraces: Southern Oregon portion of the Cascadia forearc. *Journal of Geophysical Research: Solid Earth*, *95*(B5), pp.6685-6698.

Nicholls, R.J. and Cazenave, A., 2010. Sea-level rise and its impact on coastal zones. *Science*, 328(5985), pp.1517-1520.

Omura, A. and Ota, Y., 1992. Paleo sea-level change during the last 300, 000 years deduced from the morpho-stratigraphy of coral reef terraces and 230Th/234U ages of terrace deposits. *The Quaternary Research (Daiyonki-Kenkyu)*, *31*(5), pp.313-327.

Peltier, W.R., 2004. Global glacial isostasy and the surface of the ice-age Earth: the ICE-5G (VM2) model and GRACE. *Annu. Rev. Earth Planet. Sci.*, *32*, pp.111-149.

Pico, T., Mitrovica, J. X., Ferrier, K. L., & Braun, J. (2016). Global ice volume during MIS 3 inferred from a sea-level analysis of sedimentary core records in the Yellow River Delta. Quaternary Science Reviews, 152, 72-79.

Pico, T., Creveling, J.R. and Mitrovica, J.X., 2017. Sea-level records from the US mid-Atlantic constrain Laurentide Ice Sheet extent during Marine Isotope Stage 3. *Nature communications*, *8*(1), pp.1-6.

Portenga, E.W. and Bierman, P.R., 2011. Understanding Earth's eroding surface with 10 Be. *GSA today*, *21*(8), pp.4-10.

Raymo, M. E., Mitrovica, J. X., O'Leary, M. J., DeConto, R. M., & Hearty, P. J. (2011). Departures from eustasy in Pliocene sea-level records. Nature Geoscience, 4(5), 328.

Reynolds, D.J., Steckler, M.S. and Coakley, B.J., 1991. The role of the sediment load in sequence stratigraphy: the influence of flexural isostasy and compaction. *Journal of Geophysical Research: Solid Earth*, *96*(B4), pp.6931-6949.

Rovere, A., Raymo, M.E., Mitrovica, J.X., Hearty, P.J., O'Leary, M.J. and Inglis, J.D., 2014. The Mid-Pliocene sea-level conundrum: Glacial isostasy, eustasy and dynamic topography. *Earth and Planetary Science Letters*, *387*, pp.27-33.

Rowley, D. B., Forte, A. M., Moucha, R., Mitrovica, J. X., Simmons, N. A., & Grand, S. P. (2013). Dynamic topography change of the eastern United States since 3 million years ago. Science, 340(6140), 1560-1563.

Ruetenik, G.A., Moucha, R. and Hoke, G.D., 2016. Landscape response to changes in dynamic topography. *Terra Nova*, *28*(4), pp.289-296.

Simms, A.R., Anderson, J.B., DeWitt, R., Lambeck, K. and Purcell, A., 2013. Quantifying rates of coastal subsidence since the last interglacial and the role of sediment loading. *Global and Planetary Change*, *111*, pp.296-308.

Simms, A.R., Rouby, H. and Lambeck, K., 2016. Marine terraces and rates of vertical tectonic motion: The importance of glacio-isostatic adjustment along the Pacific coast of central North America. *Bulletin*, *128*(1-2), pp.81-93.

Suppe, J., 1981. Mechanics of mountain building and metamorphism in Taiwan. *Mem. Geol. Soc. China*, *4*(6), pp.67-89.

Suppe, J., 1984. Kinematics of arc-continent collision, flipping of subduction, and back-arc spreading near Taiwan. *Memoir. Geol. Soc. China*, *6*, pp.21-33.

Szwillus, W., Ebbing, J. and Holzrichter, N., 2016. Importance of far-field topographic and isostatic corrections for regional density modelling. *Geophysical Journal International*, 207(1), pp.274-287.

Tamisiea, M.E., Mitrovica, J.X., Milne, G.A. and Davis, J.L., 2001. Global geoid and sea level changes due to present-day ice mass fluctuations. *Journal of Geophysical Research: Solid Earth*, *106*(B12), pp.30849-30863.

Teng, L.S., Lee, C.T., Tsai, Y.B. and Hsiao, L.Y., 2000. Slab breakoff as a mechanism for flipping of subduction polarity in Taiwan. *Geology*, *28*(2), pp.155-158.

Tesauro, M., Kaban, M.K. and Cloetingh, S.A., 2012. Global strength and elastic thickness of the lithosphere. *Global and Planetary Change*, *90*, pp.51-57.

Vita-Finzi, C., 2000. Deformation and seismicity of Taiwan. *Proceedings of the National Academy of Sciences*, *97*(21), pp.11176-11180.

Vita-Finzi, C. and Lin, J.C., 1998. Serial reverse and strike slip on imbricate faults: The Coastal

Range of east Taiwan. *Geology*, *26*(3), pp.279-281.

Wang, C.H. and Burnett, W.C., 1990. Holocene mean uplift rates across an active plate-collision boundary in Taiwan. *Science*, *248*(4952), pp.204-206.

Willett, S.D., Fisher, D., Fuller, C., En-Chao, Y. and Chia-Yu, L., 2003. Erosion rates and orogenic-wedge kinematics in Taiwan inferred from fission-track thermochronometry. *Geology*, *31*(11), pp.945-948.

Wu, F.T., 1978. Recent tectonics of Taiwan. *Journal of Physics of the Earth*, *26*(Supplement), pp.S265-S299.

Wolstencroft, M., Shen, Z., Törnqvist, T.E., Milne, G.A. and Kulp, M., 2014. Understanding subsidence in the Mississippi Delta region due to sediment, ice, and ocean loading: Insights from geophysical modeling. *Journal of Geophysical Research: Solid Earth*, *119*(4), pp.3838-3856.

Woo, H. B., Panning, M. P., Adams, P. N., & Dutton, A. (2017). Karst-driven flexural isostasy in North-Central Florida. Geochemistry, Geophysics, Geosystems, 18(9), 3327-3339.

Yu, S.B., Chen, H.Y. and Kuo, L.C., 1997. Velocity field of GPS stations in the Taiwan area. *Tectonophysics*, *274*(1-3), pp.41-59.

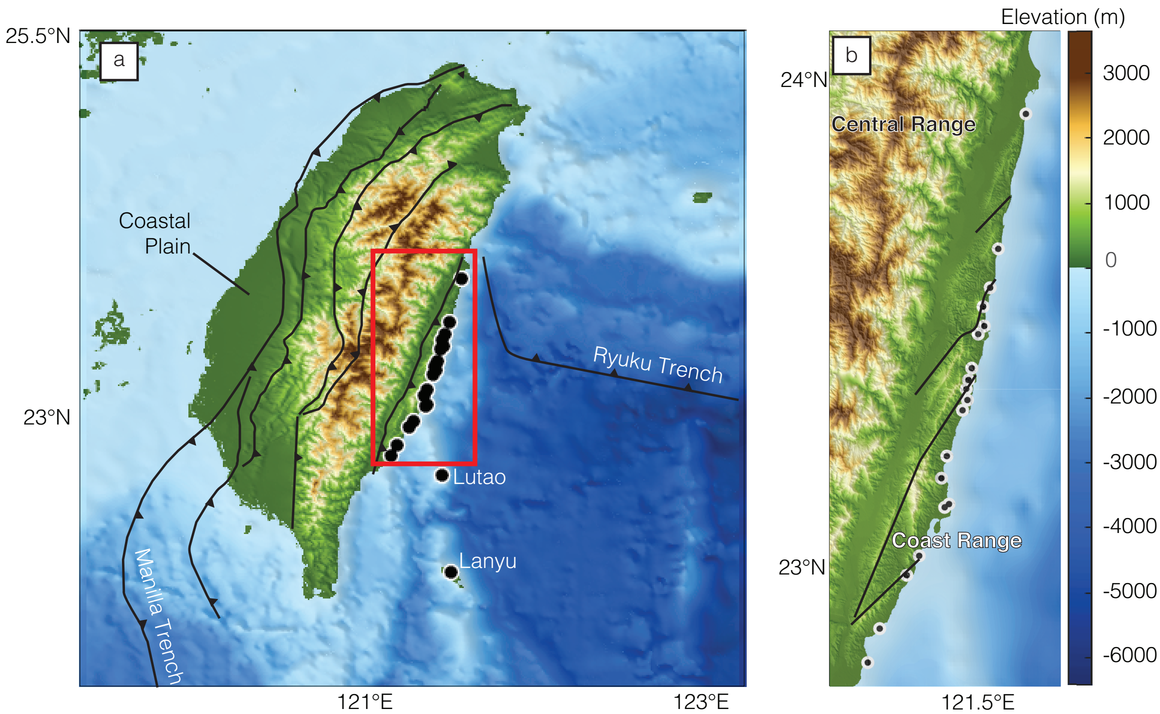

Figure 1: a) Locations of SL markers in eastern Taiwan (black circles; Table S1) and major faults after Lee et al., (2002). b) Zoomed in image of the coast range showing faults (black lines) from Vita Finzi and Lin (1998).

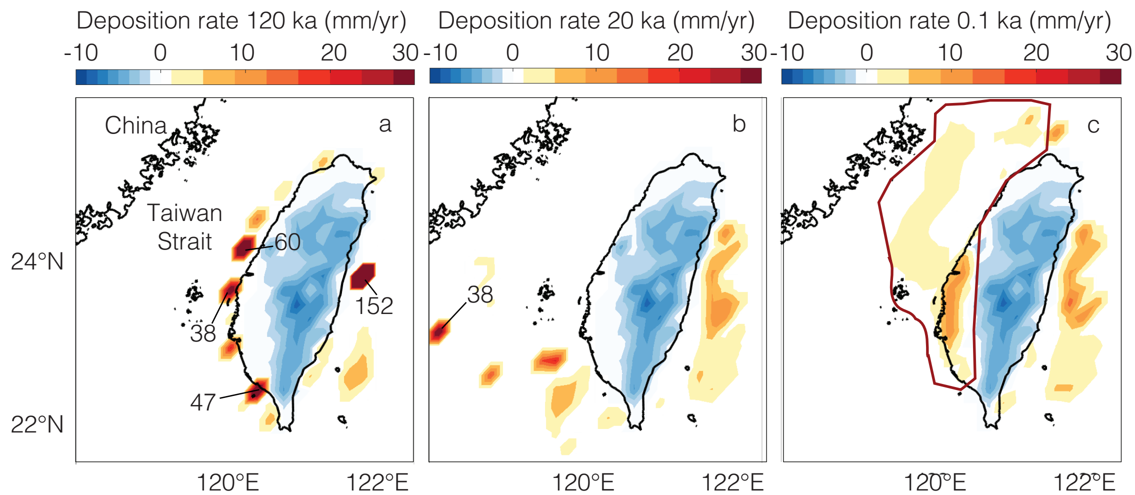

Figure 2: Snapshots of erosion rates (blue, negative values) and deposition rates (yellow to red, positive values) in Taiwan at 120 ka (panel a), 20 ka (b), and 0.1 ka (c), which are representative of the rates used to reconstruct the history of sediment redistribution over the last glacial cycle. Rates were taken from erosion rate reconstructions in Fox et al. (2014), deposition rate measurements in Liu et al. (2008), and application of the marine deposition model of Ruetenik et al. (2016). The sediment redistribution history generated from these rates was used to drive sea-level responses (Section 3.2). Labeled numbers represent deposition rates (mm/yr) for saturated values. The purple line in panel c shows the area over which the Liu et al. (2008) data were applied.

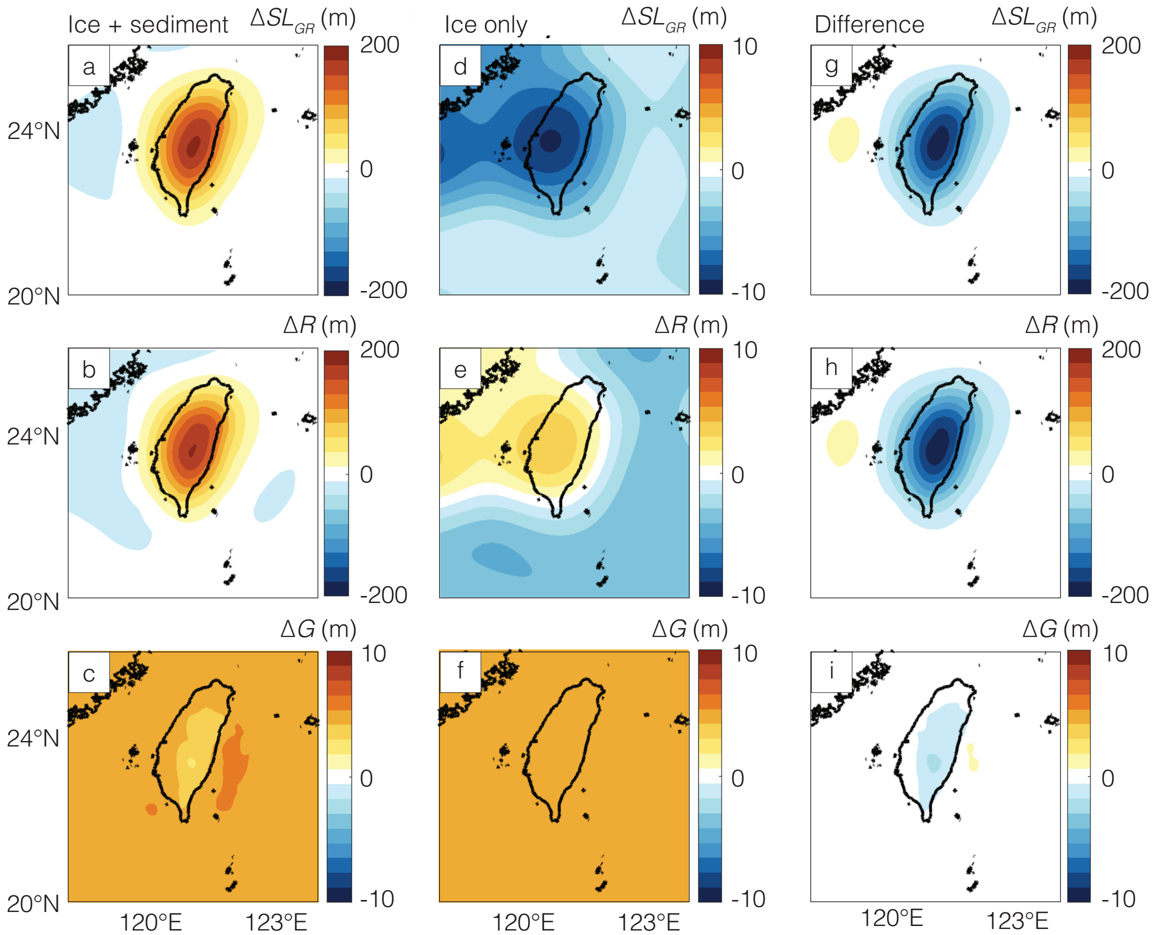

Figure 3a-c: Cumulative changes in sea level ($\Delta SL_{GR} = \Delta G - \Delta R$; panel a), crustal elevation (ΔR; panel b), and the sea-surface equipotential (ΔG; panel c) at the end of a 122-kyr simulation driven by regional sediment redistribution (Figure 2) and global ice mass changes. **d-f.** As in panels a-c, except for a simulation driven only by global ice mass changes. **g.** The difference between panels d and a isolates the net contribution of sediment redistribution to ΔSL_{GR}, and shows that these effects form a bullseye pattern around Taiwan. **h-i.** As in panel g, except for sediment's contribution to the differences in ΔR and ΔG, respectively. These show that sediment redistribution has a much larger effect on the change in sea level over this time period in Taiwan (panel g) than global ice volume changes do (panel d). Note differences in color bar scales between frames.

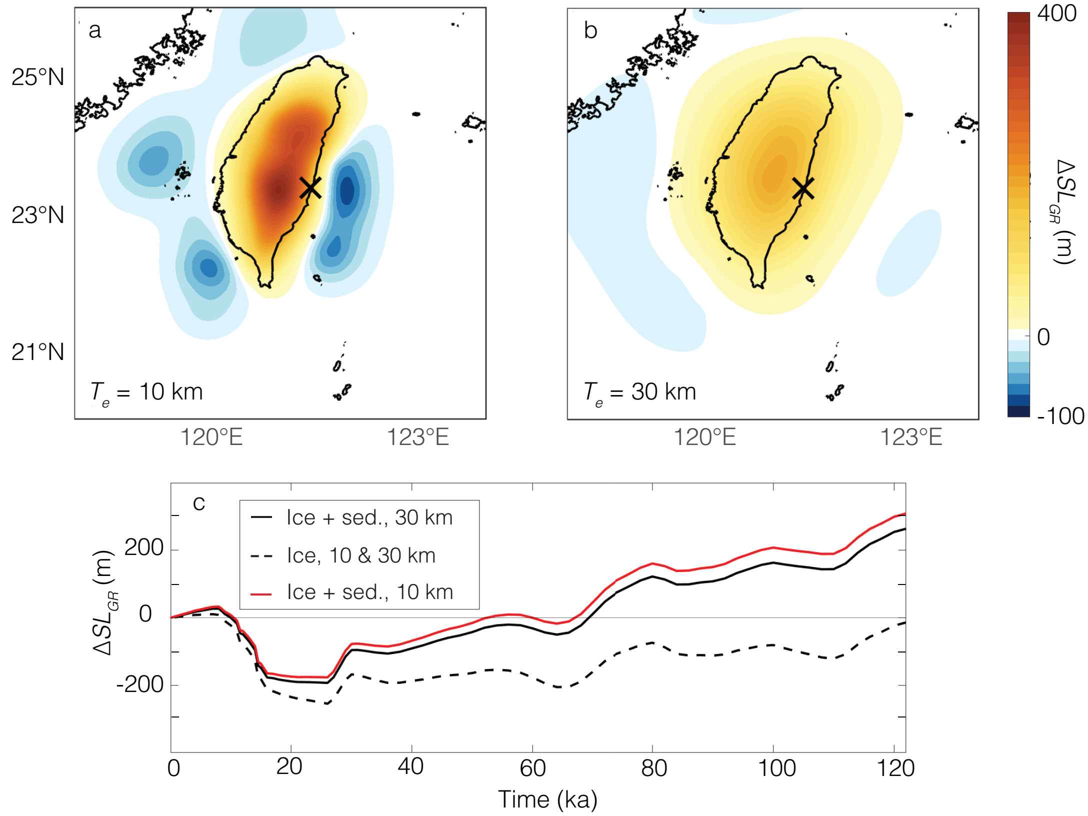

Figure 4: Sensitivity of modeled sea-level change to lithospheric effective elastic thickness. **a.** The difference in modeled sea-level change ($\Delta SL_{GR} = \Delta G - \Delta R$) at the end of two 122-kyr simulations, one driven by regional sediment redistribution and global ice variations, and the other driven only by ice (as in Figure 3g), for an Earth model with a lithospheric effective elastic thickness T_e of 10 km. **b.** As in panel a, except for an Earth model with T_e = 30 km. A comparison of panels a and b shows that sea-level responses are narrower in space and higher in amplitude at smaller T_e. **c.** Histories of modeled sea-level change at the point on Taiwan's east coast marked with a black X in panels a-b for four simulations. Two are driven by sediment redistribution and global ice changes on Earth models with T_e = 10 km (black line) and T_e = 30 km (red line). The remaining two are driven only by global ice changes with T_e = 10 km and 30 km, and overlap with each other within the width of the dashed line in panel c. The difference between the dashed line and solid lines shows that sediment redistribution can perturb LIG-age paleoshorelines by >100 m in eastern Taiwan, implying that paleoshoreline-based inferences of paleo-sea-level change may be strongly affected by sediment redistribution here.

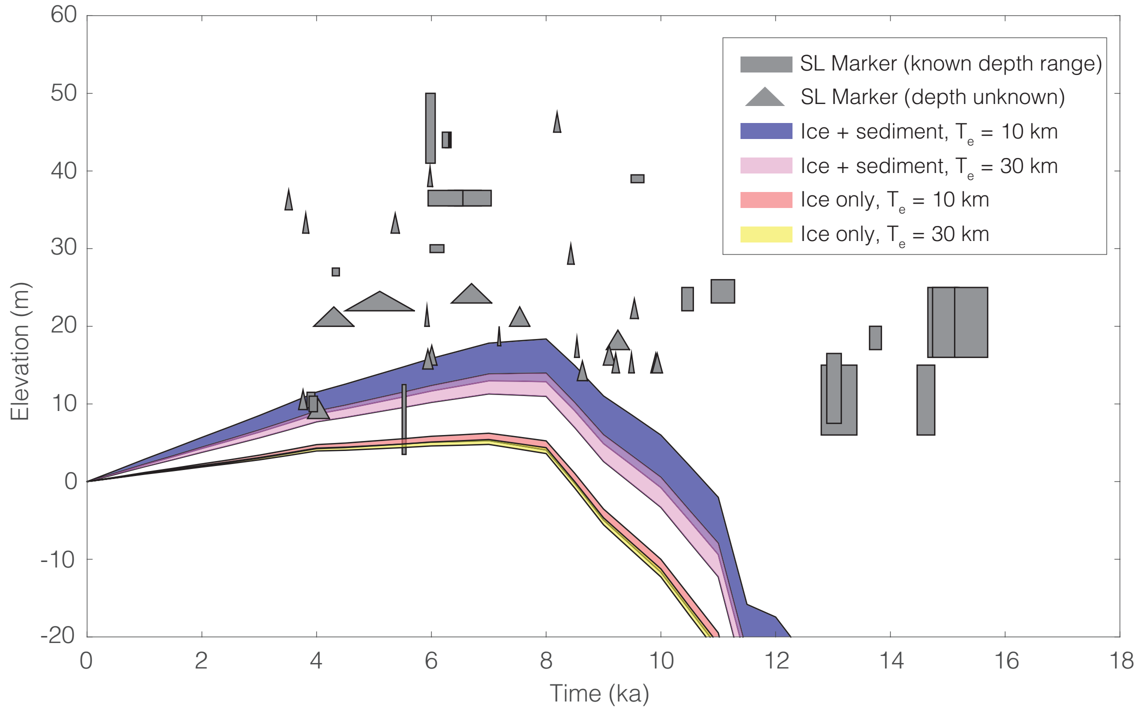

Figure 5: Observed and modeled sea-level histories on the east coast of Taiwan. Gray boxes show observed paleo-sea-level marker ages and elevations (Hsieh et al., 2004). Box widths and heights show the ranges in paleo-sea-level marker age and elevation over all localities on the east coast of Taiwan (Figure 1). Triangles represent minimum elevations where the deposited depth range is undefined, and triangle widths correspond to age ranges. Colored regions show the range in modeled relative sea level (*RSL*) among all localities along Taiwan's east coast in four simulations. Two simulations were driven by the ice and sediment variations in Section 3 (pink and purple for Earth models with T_e = 10 km and 30 km, respectively), and two simulations were driven by ice variations only (orange and yellow for T_e = 10 km and 30 km, respectively). This shows that accounting for sediment redistribution increases modeled *RSL* substantially, which brings the modeled sea-level history closer to—but generally still lower than—most of the observed paleo-sea-level markers.

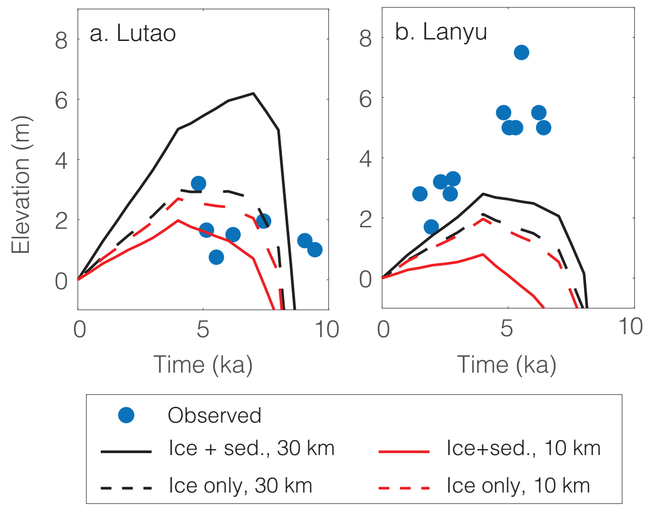

Figure 6: Comparison of observed and modeled relative sea-level histories on the islands of Lutao (panel a) and Lanyu (panel b), which lie ~30 km and ~65 km east of Taiwan, respectively (Figure 1). Blue dots show elevations and ages of paleo-sea-level markers. Lines show modeled *RSL* histories in simulations driven by sediment and ice variations (solid lines) and only ice variations (dashed lines) for Earth models with T_e = 30 km (black) and T_e = 10 km (red). These show that sediment redistribution in Taiwan is capable of significantly affecting sea-level changes at sites >60 km away from Taiwan. The difference between the SL10 and SL30 simulations illustrate the effects of lithospheric thickness on modeled *RSL* and hence elevation differences between observed paleoshorelines and modeled *RSL*.

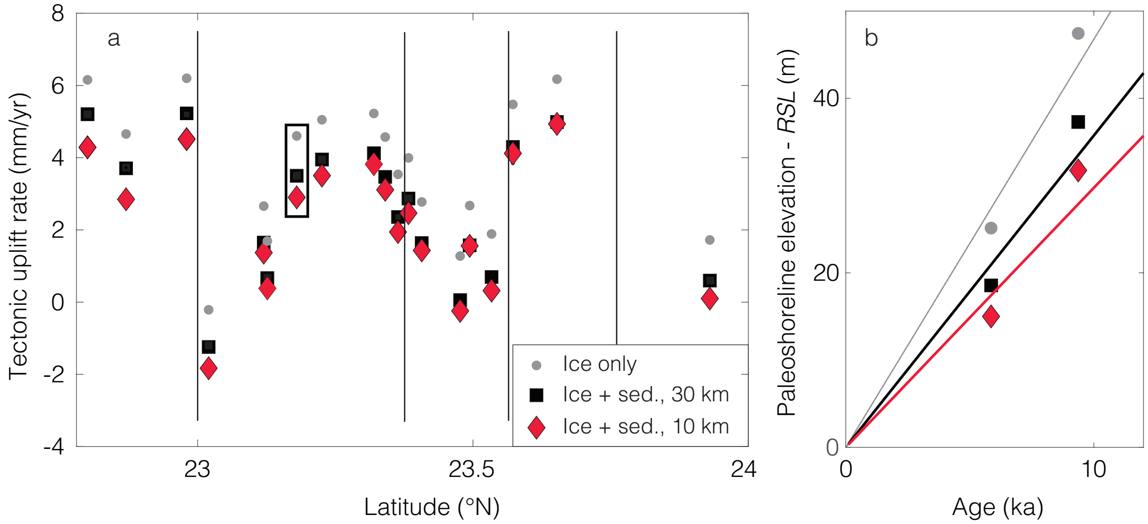

Figure 7a: Estimates of tectonically driven rock uplift rates, $U_{tectonic}$, along Taiwan's east coast. These are inferred from residuals between observed paleoshoreline elevations and modeled sea-level changes (Figure 5). Vertical lines indicate locations of inferred fault (Vita-Finzi and Lin, 1998). Inferred tectonically driven uplift rates are systematically smaller in simulations driven by both sediment and ice, indicating that estimates of tectonically driven uplift rates on Taiwan's east coast would be overestimated if sediment redistribution were not accounted for. **b.** An example of how the uplift rates in panel a were calculated. All rates were determined from the slope of a linear regression between paleo-sea-level marker age and the difference between the paleo-sea-level elevation and modeled *RSL*. Here, the data correspond to the rates in panel a at 23.18°N. Gray circles represent ages and residual elevations inferred from sea-level simulations driven only by global ice variations. Red diamonds and black squares represent ages and residual elevations inferred from simulations driven by both sediment and ice variations in Earth models with 10-km and 30-km effective elastic lithospheric thicknesses, respectively.